Journal of Biomedical Optics

BiomedicalOptics.SPIEDigitalLibrary.org

Quantitative investigation of red blood cell three-dimensional geometric and chemical changes in the storage lesion using digital holographic microscopy

Keyvan Jaferzadeh
Inkyu Moon

SPIE.

Quantitative investigation of red blood cell three-dimensional geometric and chemical changes in the storage lesion using digital holographic microscopy

Keyvan Jaferzadeh and Inkyu Moon*
Chosun University, Department of Computer Engineering, 309 Pilmun-daero, Dong-gu, Gwangju 501-759, Republic of Korea

Abstract. Quantitative phase information obtained by digital holographic microscopy (DHM) can provide new insight into the functions and morphology of single red blood cells (RBCs). Since the functionality of a RBC is related to its three-dimensional (3-D) shape, quantitative 3-D geometric changes induced by storage time can help hematologists realize its optimal functionality period. We quantitatively investigate RBC 3-D geometric changes in the storage lesion using DHM. Our experimental results show that the substantial geometric transformation of the biconcave-shaped RBCs to the spherocyte occurs due to RBC storage lesion. This transformation leads to progressive loss of cell surface area, surface-to-volume ratio, and functionality of RBCs. Furthermore, our quantitative analysis shows that there are significant correlations between chemical and morphological properties of RBCs. [DOI: 10.1117/1.JBO.20.11.111218]

Keywords: three-dimensional image processing; digital holographic microscopy; quantitative phase imaging; cell morphology analysis; red blood cell analysis.

Paper 150212SSRR received Apr. 7, 2015; accepted for publication Sep. 22, 2015; published online Oct. 21, 2015.

1 Introduction

In the human body, red blood cells (RBCs) serve many purposes, but one of the most important functions of RBCs is to transport oxygen and carbon dioxide between the lungs and the rest of the body's tissues. Every aspect of a RBC, including metabolism, size, and shape, is adapted to maximize functionality. Importantly, the RBC's shape should be optimal for maximal deformation, maximum surface at a given volume, rapid changes, and survival of the cell during its many repeated passages through the narrow channels. In fact, surface area is one of the most important properties of RBCs, since the exchange of oxygen and carbon dioxide takes place at their surface; larger surface area allows for an increased exchange of oxygen and carbon dioxide in the lungs and within the body cells. These conditions are satisfied by a biconcave disk shape, which is considered the medical norm for RBCs.[1] The biconcave RBC has a flexible membrane with a high surface-to-volume ratio (SVR) that facilitates large, reversible, elastic deformation of the RBC as it repeatedly passes through small capillaries during microcirculation.[2] In particular, the biconcave shape of RBCs is regarded as the result of minimizing the free energy of membranes under area and volume constraints, since there are no complex inner structures within RBC.[3] However, during the storage period, RBCs and their preservative media suffer metabolic, biochemical, biomechanical, and molecular changes, commonly referred to as storage lesions.[4] Furthermore, a large range of adverse effects related to RBC storage have been reported in critically ill patients when the RBC storage period exceeds 4 weeks. These effects include increased mortality, nosocomial infections, multiple organ failure, renal failure, and deep vein thrombosis.[5,6] Much scientific evidence, however, supports that during the storage period, the RBC structure undergoes essential changes in shape: from biconcave disc to flat disk, and finally to a spherocyte, which leads to the inability of the RBCs to carry oxygen.[7–10] Although a number of studies in recent years have analyzed changes in RBCs throughout their lifespan, most have not specified accurate quantitative morphological and surface-to-volume rate-related changes, which are considered vital in terms of the performance of RBCs.

Conventional two-dimensional microscopic systems suffer from losses of quantitative information regarding the morphological properties of transparent or semitransparent microscopic samples. Indeed, capturing detailed surface area and volume data is impossible with these systems. Digital holographic microscopy (DHM) is a promising tool in this regard; it allows for real-time three-dimensional (3-D) cell imaging due to its capability of noninvasively visualizing and quantifying transparent biological cells.[11–22] This DHM technique has been utilized in studies of various kinds of cells such as protozoa, bacteria, plant cells, blood cells, nerve cells, and stem cells without labeling.[23] Recently, it has been demonstrated that the RBC quantitative phase image obtained by DHM enables the measurement of characteristic properties, such as mean corpuscular volume, projected surface area (PSA), mean corpuscular hemoglobin (MCH), and MCH surface density, of RBCs with different storage periods.[24] Kim et al.[25] demonstrated that the correlation analysis of these RBC parameters provides unique information for distinguishing and understanding blood diseases. Bhaduri

*Address all correspondence to: Inkyu Moon, E-mail: inkyu.moon@chosun.ac.kr

1083-3668/2015/$25.00 © 2015 SPIE

et al.[26] analyzed morphological and deformation changes of discocyte-shaped RBCs during storage lesion utilizing topography with nanometer sensitivity. They reported that the fluctuations rate for discocyte-shaped RBCs decreases while cells are aging in blood banks. However, chemical parameters, such as MCH, do not change during the same period.[26] Even with this technique, the questions related to the quantitative morphological changes of RBCs in storage lesion remain unanswered and require further investigation.

In this paper, the morphological and chemical parameters of individual RBCs are simultaneously obtained by using noninvasive and label-free DHM technique. The morphological and chemical parameters of RBCs in single-cell level with different ages are automatically quantified. We investigate 3-D geometric features of RBCs including surface area, sphericity index, morphological functionality factor, sphericity coefficient, and SVR in storage lesion. In addition, the correlation analysis between chemical parameters of MCH/MCH concentration and morphological parameters of RBCs in different ages is presented.

The datasets utilized for our study consist of healthy blood samples stored for 8, 13, 16, 23, 27, 30, 34, 37, 40, 47, and 57 days and are divided into 11 classes of RBCs stored in 11 different periods. The 11 classes, overall, have more than 3300 RBCs, with more than 300 RBCs per each class. To calculate 3-D geometric parameters of RBCs, a marker-controlled watershed segmentation algorithm[27] is utilized, which removed the unnecessary background, segmenting reconstructed images into many single RBCs. Finally, morphological and chemical parameters of each single RBC for the various storage times are calculated, and the results are compared against each other. Our findings show that in storage lesion, the structure of an RBC goes through essential changes in terms of shape, i.e., from a biconcave disc to a spherocyte. Interestingly, our experimental results indicate that the surface area values of normal RBCs obtained through DHM approximately agree with the values reported by other methods.[28–30] These experimental results can contribute to the understanding of the changes in 3-D geometric features of RBCs during the storage period and can provide quantitative information to support the work of hematologists.

2 Quantitative Analysis of Red Blood Cell Three-Dimensional Geometric Changes

For the quantitative analysis of RBC 3-D geometric changes in storage lesion, off-axis DHM reconstructs the RBC phase images using the numerical algorithm described in Refs. 31–33. The schematic of the off-axis DHM is illustrated in Fig. 1. As shown in Fig. 1, the off-axis hologram between the reference beam originated from a laser and the object beam diffracted by the RBC sample through a microscope objective is recorded on the CCD camera. In our configuration, the laser source's wavelength is 682 nm and the magnification factor and the field of view for microscope are 40× and 150 μm, respectively.

In order to analyze the changes in the 3-D geometric quantities of RBCs as the storage time increases, the off-axis DHM reconstructs quantitative phase images of the 11 classes of blood samples stored for 8, 13, 16, 23, 27, 30, 34, 37, 40, 47, and 57 days, respectively.[24] The reconstructed phase image for each class includes many RBCs; however, only single cells are considered here. Then, a marker-controlled watershed segmentation algorithm[27] is applied to extract the phase data for

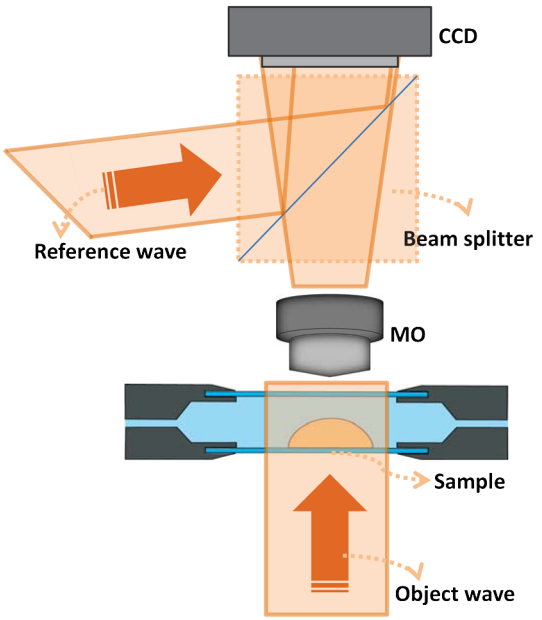

Fig. 1 Schematic of the off-axis digital holographic microscopy (DHM).

individual RBC's. Converting these phase images to thickness images will result in easier morphological computation. Accordingly, the thickness value $h(i,j)$ for each pixel of (i,j) with phase value $\varphi(i,j)$ in a phase image can be expressed as follows:[34]

$$h(i,j) = \frac{\varphi(i,j) \times \lambda}{2\pi(n_{\mathrm{rbc}} - n_{\mathrm{m}})}, \tag{1}$$

where λ is the wavelength of light source, $\varphi(i,j)$ is the phase value in radians, and the refractive index of RBCs, n_{rbc}, has been measured with a dual-wavelength DHM.[35] Here, n_{rbc} is 1.396 with no significant difference between groups of different ages. The index of refraction of the high-efficiency particulate air (HEPA) medium, n_{m}, is 1.3334. To characterize the 3-D geometric quantities of RBCs at different storage periods, a sphericity coefficient k, a ratio of the RBC thickness at the center d_{c} to the thickness at half of its radius d_{r} (dimple area), is determined as follows:[36]

$$k = \frac{d_{\mathrm{c}}}{d_{\mathrm{r}}}. \tag{2}$$

The sphericity coefficient k can determine three types of RBCs. A value of k less than unity leads to biconcave-shaped RBC, a value around unity denotes a flat disk-shaped RBC, and a value greater than unity specifies a spherocyte. A k factor of around 0.35 has been reported for healthy RBCs and around 1.12 for the sick ones.[36]

Surface area is the area of a surface or collection of surfaces bounding a solid. There are different formulas for calculating the surface area of regular shapes. Generally, the surface area with the form of a function $z = f(x,y)$ can be calculated as follows:

$$\text{Surface area} = \iint_S \sqrt{\left(\frac{\partial z}{\partial x}\right)^2 + \left(\frac{\partial z}{\partial y}\right)^2 + 1}\,\mathrm{d}A, \tag{3}$$

where the integral is taken over the entire surface.[37] For irregular shapes, like the ones of RBCs, however, many methods have

been proposed.[38] These methods typically split and divide irregular surfaces into smaller regular areas and add these smaller areas to give the entire surface area. Understandably, the accuracy of such a calculation is dependent on the smaller area chosen. In most cases, covering the entire surface area of an RBC by small triangles can provide a high accuracy (error is less than 5%). The surface area of any of these triangles can be calculated easily by some popular methods, such as the Heron formula, which uses the length of each side of a triangle, using the base and height side, using one side of an equilateral triangle, or using the lengths of two sides and the included angle. If we have a triangle whose sides have lengths a, b, and c, the Heron formula states that

$$\text{Surface area} = \sqrt{s(s-a)(s-b)(s-c)}, \tag{4}$$

where s is $(a+b+c)/2$. In this paper, the surface area of each triangle is calculated by Eq. (3). Our experimental results show that Eq. (3) is accurate enough for the RBC surface area calculation. The total surface area of an RBC in DHM consists of the surface area of the top view summed with the PSA of the top view. The PSA is defined as follows:[24]

$$\text{PSA} = Np^2, \tag{5}$$

where p denotes the pixel size in the DHM phase image (here $p = 0.159$ μm) and N is the total number of pixels within an RBC. PSA is reported to be around 45 ± 5 μm^2 for normal RBCs[24] and can also be used to estimate the radius of an RBC.

The RBC radius (r) can be estimated here by considering the radius of a circle having the area of the PSA of a RBC:

$$r \cong \sqrt{\frac{\text{PSA}}{\pi}}. \tag{6}$$

The surface area for the top view of an RBC (see Fig. 2) can be computed by different methods; for the purpose of our study, the top view is partitioned into small triangles as mentioned earlier, and a summation of the areas of all the small triangles determines the surface area of the top view. Accordingly, the total surface area of a single RBC can be computed as follows:

$$\text{SA} = \text{PSA} + \text{TVSA}, \tag{7}$$

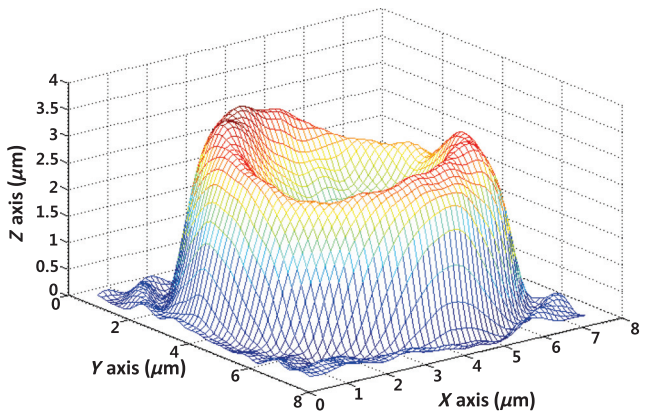

Fig. 2 Three-dimensional (3-D) view of a red blood cell (RBC) obtained by the DHM method.

where PSA is the projected surface area and TVSA is the surface area of the top view. With the calculated surface area for an RBC, we can estimate the morphological functionality factor of the erythrocyte f, which is the ratio of the RBC surface area to the surface area of a spherocyte with the same volume:[36]

$$f = \frac{\text{SA}}{S_\text{s}} = \frac{\text{SA}}{4\pi r^2}, \tag{8}$$

where SA can be calculated by Eq. (7) and S_s is the surface area of the sphere with radius r. An f value around unity characterizes a spherocyte. Moreover, taking into consideration Eq. (7), we can calculate the total surface area of all RBCs S_t, which determines oxygen capacity of blood. The S_t is equal to the product of the number of RBCs in blood M and the arithmetic mean surface area SA_m of RBCs:[36]

$$S_\text{t} = M \times SA_\text{m}. \tag{9}$$

Equation (7) can be applied to obtain the SVR, which is a critical parameter for an RBC because the higher the SVR, the more material a cell can exchange with its surroundings. According to Ref. 39, the volume of RBC in a DHM phase image is denoted as

$$V \cong \frac{p^2\lambda \sum_{i=1}^{k}\sum_{j=1}^{l}\varphi(i,j)}{2\pi(n_\text{rbc} - n_\text{m})}, \tag{10}$$

where p denotes the pixel size in the DHM phase image, k and l are the width and height of the phase image, λ is the wavelength of the light source, $\varphi(i,j)$ is the phase value in radians, and refractive indices n_rbc and n_m are 1.396 and 1.3334, respectively.

Another important parameter related to the shape of the RBCs is the sphericity index (dimensionless), which indicates to what extent the shape of a cell approaches a sphere. The sphericity index of each cell determines the degree of tolerance of that cell to deformation, for example, in passing through a narrow cylindrical channel.[40] This parameter, also, can be useful in discriminating between healthy and pathological cells, for example, in identifying pathological cells in some hereditary diseases like spherocytosis.[40] Deformability of RBCs can also be identified by measuring RBC mechanical parameters of fluctuations rate and shear stress.[41] Utilizing DHM technology, it has been shown that the deformability of RBCs gradually decreases as cells are aging.[26] Thus, a determination of RBC deformability is the sphericity index, defined as follows:

$$\text{SP} = \frac{4\pi V^{2/3}}{(4\pi/3)^{2/3}\text{SA}}. \tag{11}$$

The mean value of the sphericity index of normal RBCs has been reported to be 0.79 ± 0.026 at room temperature using interference microscopy.[42] A similar value (0.73 ± 0.02) has also been obtained using a micropipetting method.[30] According to Eq. (11), the sphericity index has a maximal value of unity, which corresponds to a spherical cell.

3 Experimental Results and Discussion

The original RBCs were donated by healthy people and were stored in a transfusion bag. These RBCs were obtained from the Service Régional Vaudois de Transfusion Sanguine in Switzerland. The RBCs were stored at 4°C during the storage

period. The RBC concentrate was extracted from the blood transfusion bag and diluted in HEPA buffer (15-mM HEPES pH 7.4, 130-mM NaCl, 5.4-mM KCl, 10-mM glucose, 1-mM $CaCl_2$, 0.5-mM $MgCl_2$, and 1-mg/mL bovine serum albumin) at a concentration of approximately 0.15%. Then, 0.2 mL of the RBC suspension were introduced into the experimental chamber, which itself consisted of two coverslips separated by spacers 1.2-mm thick. In order to allow for the sedimentation of the cells on the bottom coverslip, cells were incubated for 30 min at a temperature of 37°C before mounting the chamber on the DHM stage. All experiments were conducted at room temperature.

After segmenting and extracting the RBCs from the quantitative phase images, the surface area, volume, SVR, morphological functionality factor f, cell diameter, sphericity coefficient k, sphericity index SP, and oxygen capacity S_t for all samples in the storage time as well as standard deviations were calculated. To reduce noise and increase the accuracy in Eq. (2), d_c and four adjacent values were averaged; d_r is the average of the some values (each one was chosen from a different portion of dimple). Table 1 shows the calculated mean and standard deviation for all the 3-D geometric properties of RBCs with different ages.

Figure 3 shows the graphical representation of the central tendency of the RBCs' 3-D geometric properties with different ages. Figures 4 and 5 show some RBC samples at different storage times and their respective surface area's histograms. It shows the variation in size and shape of RBCs stored. As shown in Figs. 4 and 5, the leftward shift of the normal distribution for the surface area implies that RBC's surface area is dropping while storage time is increasing. Considering Table 1 and Figs. 3–5, though the surface area fluctuating during the first 4 weeks of the storage period, almost immediately after it begins to drop. The same trends that were identified for changes in cell area against aging are also similar for the cell diameter. In contrast, at these times, volume is only changing with slight fluctuations.[24] As the diameter decreases under almost fixed volume, the thickness value is increasing, which is consistent with previous findings.[24] In Ref. 34, the cell diameter for healthy RBCs was reported to be 7.7 ± 0.5 μm; however, while the cell diameter for the first 5 weeks is within this reported range, it begins to decrease when the storage time exceeds 5 weeks. It is interesting to note that the RBC surface area values within the first four weeks of the storage period, reported in Table 1, are close to those obtained by other methods.[28–30] Also, we note that the surface area for the top view of the cell neither decreases nor increases significantly and remains within its standard deviation across the entire storage period, while the PSA drops as the storage time increases.

Table 1 Three-dimensional (3-D) geometric quantities of RBC in different storage days estimated by our proposed method.

		Storage time (days)										
Property		8	13	16	23	27	30	34	37	40	47	57
Projected surface area (PSA) (μm^2)	Mean	45	46	47	45	47	42	43	41	39	34	26
	STD	5	6	7	7	10	8	9	8	9	9	6
Top-view surface area (TVSA) (μm^2)	Mean	81	81	89	83	84	85	84	81	81	79	81
	STD	8	8	9	8	8	9	7	6	8	8	10
Surface area (μm^2)	Mean	126	127	136	128	131	127	127	122	120	113	107
	STD	11	14	16	16	17	16	11	12	13	14	15
Volume (μm^3)	Mean	91	92	102	94	98	88	86	93	98	98	94
	STD	9	12	14	14	15	20	12	11	12	13	11
Surface-to-volume ratio (SVR) (μm^{-1})	Mean	1.38	1.38	1.33	1.36	1.34	1.44	1.48	1.31	1.22	1.15	1.13
	STD	0.19	0.22	0.19	0.20	0.21	0.26	0.21	0.22	0.20	0.20	0.16
Cell diameter (μm)	Mean	7.76	7.77	7.76	7.63	7.70	7.45	7.65	7.52	7.25	6.73	6.04
	STD	0.49	0.55	0.53	0.58	0.58	0.69	0.75	0.75	0.86	0.89	0.68
k factor	Mean	0.88	0.78	0.66	0.84	0.70	0.70	0.93	0.93	1.03	1.20	1.35
	STD	0.18	0.19	0.21	0.22	0.23	0.37	0.30	0.56	0.34	0.36	0.41
f factor	Mean	0.66	0.69	0.72	0.70	0.70	0.73	0.69	0.69	0.73	0.79	0.93
	STD	0.07	0.09	0.10	0.10	0.10	0.13	0.17	0.14	0.15	0.16	0.16
Sphericity index	Mean	0.78	0.78	0.78	0.78	0.79	0.75	0.74	0.81	0.86	0.91	0.94
	STD	0.07	0.08	0.07	0.08	0.07	0.08	0.08	0.09	0.09	0.10	0.09

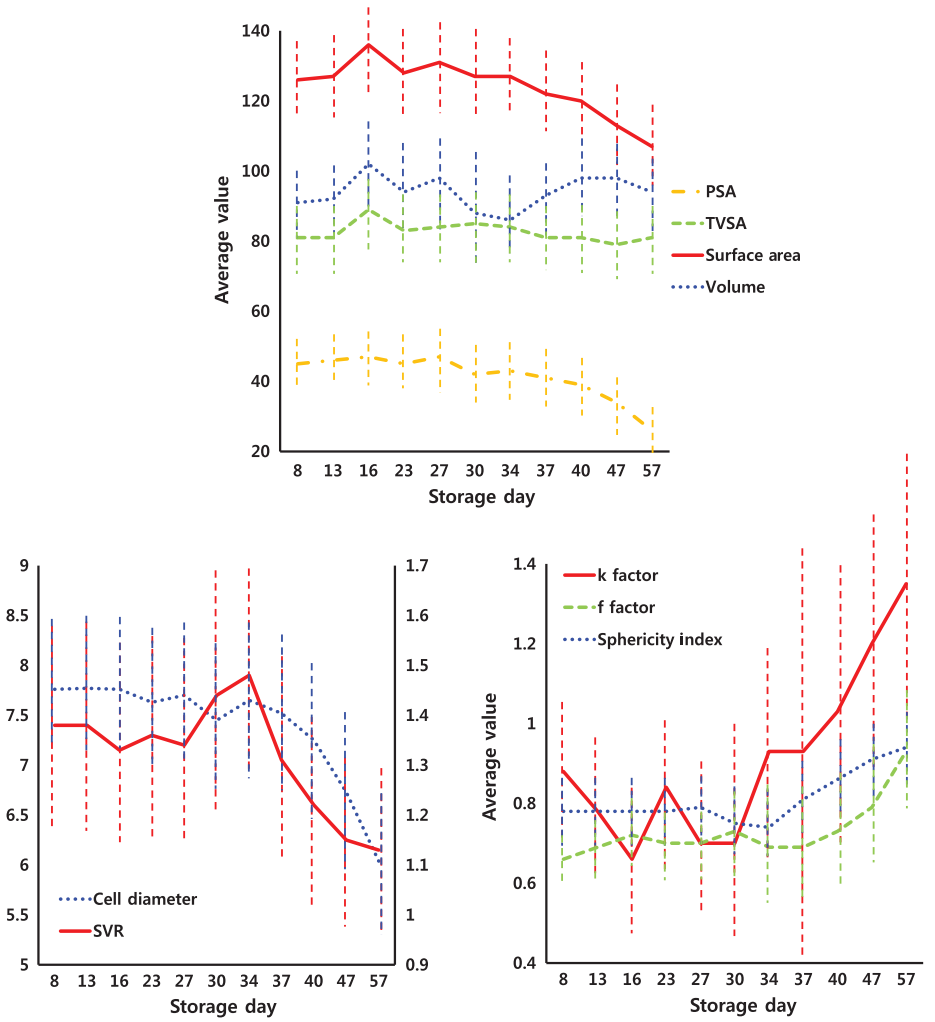

Fig. 3 Graphical representation of the central tendency of the RBC's projected surface area (PSA), top-view surface area (TVSA), surface area, volume, cell diameter, surface-to-volume ratio (SVR), *k* factor, *f* factor, and sphericity index with different ages. Bar is the standard deviation.

The SVR, which is an important characteristic for RBCs, is decreasing, since its volume remains relatively constant while its surface area is dropping. Most biological cells maximize the SRV to preserve their biological processes. It is noted that the SVR in the RBC within the first 4 weeks of storage is approximately 1.36. As mentioned previously, aside from the presence of hemoglobin, the cell surface area or SVR is the most important factor in the oxygen-carrying processes of erythrocytes. The effect of a smaller available surface area is clearly seen in terms of the oxygen capacity, which can be estimated using the averaged surface area values for different storage periods according to Eq. (9). We found that the oxygen capacity for RBCs within a 30-day storage period is approximately 15% larger than that for RBCs with a storage period over 6 weeks, assuming an equal number of RBCs for each storage day.

The k factor (sphericity coefficient) starts from a value less than 1 and increases gradually to a value greater than 1. This means RBCs are biconcave initially and as storage time exceeds 5 weeks, they become flat disks and finally transform into spherocytes. In contrast, the functionality factor f has the same trend as the sphericity coefficient in the way that f approaches unity. This means that the surface area of RBCs is almost equal to a sphere having the same radius. The sphericity index, which determines deformability, has the same trend as the functionality factor and the sphericity coefficient, since it rises after the first 5 weeks of storage. Our findings about sphericity index suggest that during storage time, sphericity index rises, which imply less tolerance during passing through narrow channels.

Modifications in the morphological functionality factor f, along with the sphericity coefficient k, consistently show that RBCs transform from biconcave into spherocyte under the constant volume. Regarding these substantial changes, the surface area and the SVR are decreasing, which causes a decrease in the functionality with respect to materials exchange between the tissues and lungs.

The morphological functionality factor f, sphericity coefficient k, and sphericity index are very important since they can specify the shape, type, and deformability of RBCs under aging. An increase in the sphericity coefficient corresponds to a decrease in the surface area of the RBC under its given volume. The geometric modifications related to the decrease in the RBC's surface area cause a decrease in the functionality with respect to the oxygen supply of tissues and organs. Variations in k in the first 5 weeks of the storage period may have been due to either inaccuracies in finding the accurate values of r_c and r_d, although some pixels were averaged, or

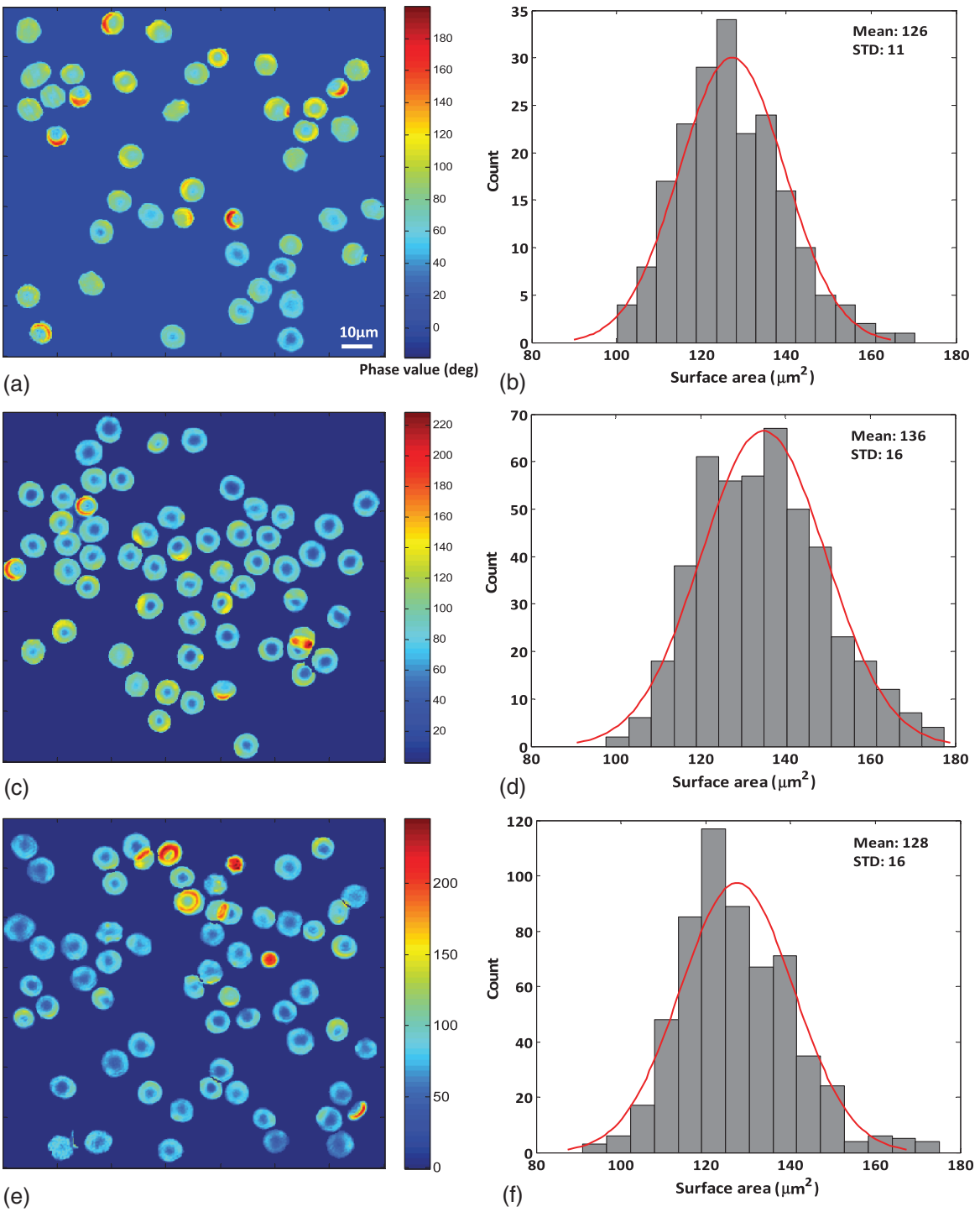

Fig. 4 Histograms of RBC surface area for different storage times: (a), (c), and (e) RBCs with 8, 16, and 23 days of storage, respectively; and (b), (d), and (f) the corresponding surface areas' histograms for each storage time.

existence of stomatocyte RBCs. In many studies, it has been established that the normal RBCs (biconcave) undergo transformations in shapes toward stomatocytes upon variations in some of their chemical components; for example, increases in the medium's pH and additions of amphiphiles or even changes in temperature.[43] A morphological functionality factor f close to unity confirms that the surface area of an RBC is almost equal to the surface area of a sphere having the same radius. Findings about k and f are consistent in this paper, and both demonstrate that RBCs are becoming flat disks and finally transforming into spherocytes. The sphericity index, which determines the degree of tolerance of a cell to deformation, is increasing, meaning that the deformability in passing through a very narrow cylindrical channel is decreasing.

The promising ability of DHM technique is not only limited to measure 3-D geometrical parameters but also allowed us to

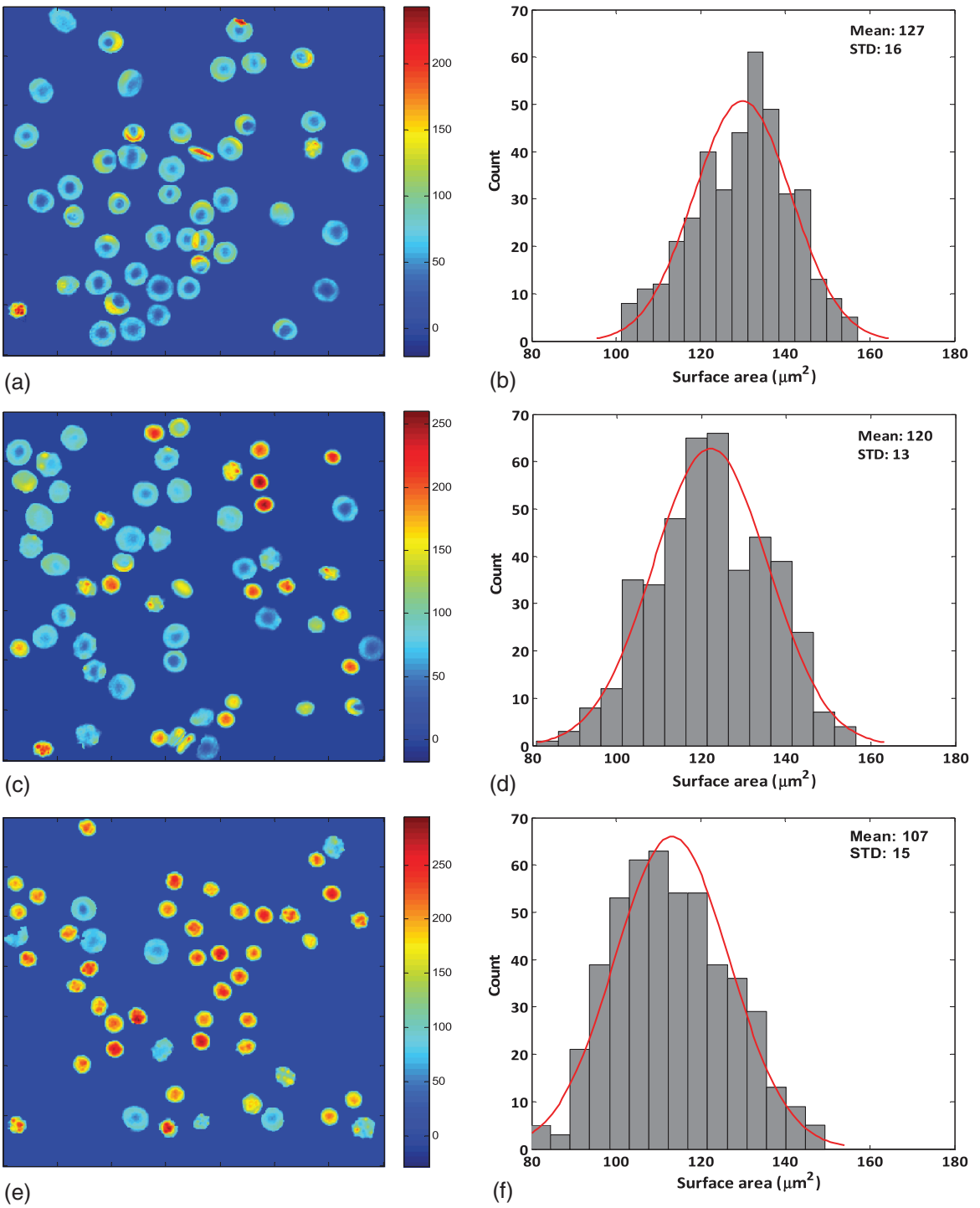

Fig. 5 Histogram of RBC surface area for different storage times: (a), (c), and (e) RBCs with 30, 40, and 57 days of storage, respectively; and (b), (d), and (f) the corresponding surface areas' histograms for each storage time.

measure the MCH of RBCs.[44] The MCH concentration (MCHC), a measure of the concentration of hemoglobin in a given volume, can be measured as follows:

$$\mathrm{MCHC} = \frac{\mathrm{MCH}}{\mathrm{MCV}}. \tag{12}$$

It turns out that MCH and MCHC do not have significant changes during the storage time changes. They just fluctuate around their mean value. Our results indicate that, while cells can undergo morphological changes during storage, they do not lose hemoglobin into the storage solution.[26] Since the chemical and morphological parameters of RBCs are measured simultaneously at the single-cell level by using DHM, we can evaluate correlation analysis between these parameters. We divided our samples into two different groups according to their storage time for the sake of clear visualization. Former contains two classes of 8 and 30 days, and latter includes 47 and 57 days

DHM data. Figure 6 presents the correlation analysis results between the morphological and chemical parameters of the groups. The correlations between the RBC parameters enable understanding of the cellular physiology of RBCs in detail.

As shown in Fig. 6, it is noted that there is a positive correlation between MCH and surface area [Fig. 6(a)] and a significantly strong positive correlation between MCH and volume [Fig. 6(b)] consistent to the previous finding.[45,46] It is worth to say that the correlation coefficient has small fluctuations and the slope of regression line changes in the stored lesion. It is interesting to observe that RBCs with higher MCHC exhibited lower values in their surface areas and volumes [Figs. 6(e) and 6(f)] in all ages, which is consistent with the previous research undertaken for populated cells.[25] Note that the correlation coefficient of surface area and MCHC value is smaller than the respective volume and MCHC at the same time. Moreover, our analysis shows that there is no significant correlation between functionality factor-MCH and functionality factor-MCHC while RBCs are aging. Furthermore, it turns out that the sphericity index follows the same trend of functionality factor similar to the previous finding.[25] Interestingly, RBCs with higher MCH exhibited lower values in their SVRs in all ages [Fig. 6(c)]. However, higher MCHC RBCs exhibit higher values in their SVR [Fig. 6(d)]. It is worth mentioning that in all cases, there are linear relationships between two variables according to the calculated root mean squared error (RMSE) of residuals values. However, we found that the RMSE of polynomial line of degree 2 for SVR-MCHC is significantly lower than that of the linear relationship.

We also calculated the correlation coefficient between the RBCs' geometrical parameters, which could enable us into a better understanding of storage lesion. Table 2 shows the correlation results between the RBCs' geometrical parameters. These correlation results demonstrate that there is a significant positive correlation between volume-diameter and surface area-diameter. We also realized that the correlation between surface area and diameter is more significant compared with the correlation between volume and diameter. In addition, we found that the surface area and volume have significant positive correlation, which implies that the cells with higher volume can have bigger surface area. Interestingly, when storage time is 57 days, we can see that the correlation coefficient between volume and surface area is higher than other days (see Table 2).

The biconcave shape allows the RBCs sufficient surface area for exchanging metabolic products across the membrane and cytoskeleton and results in their slight deformation. The

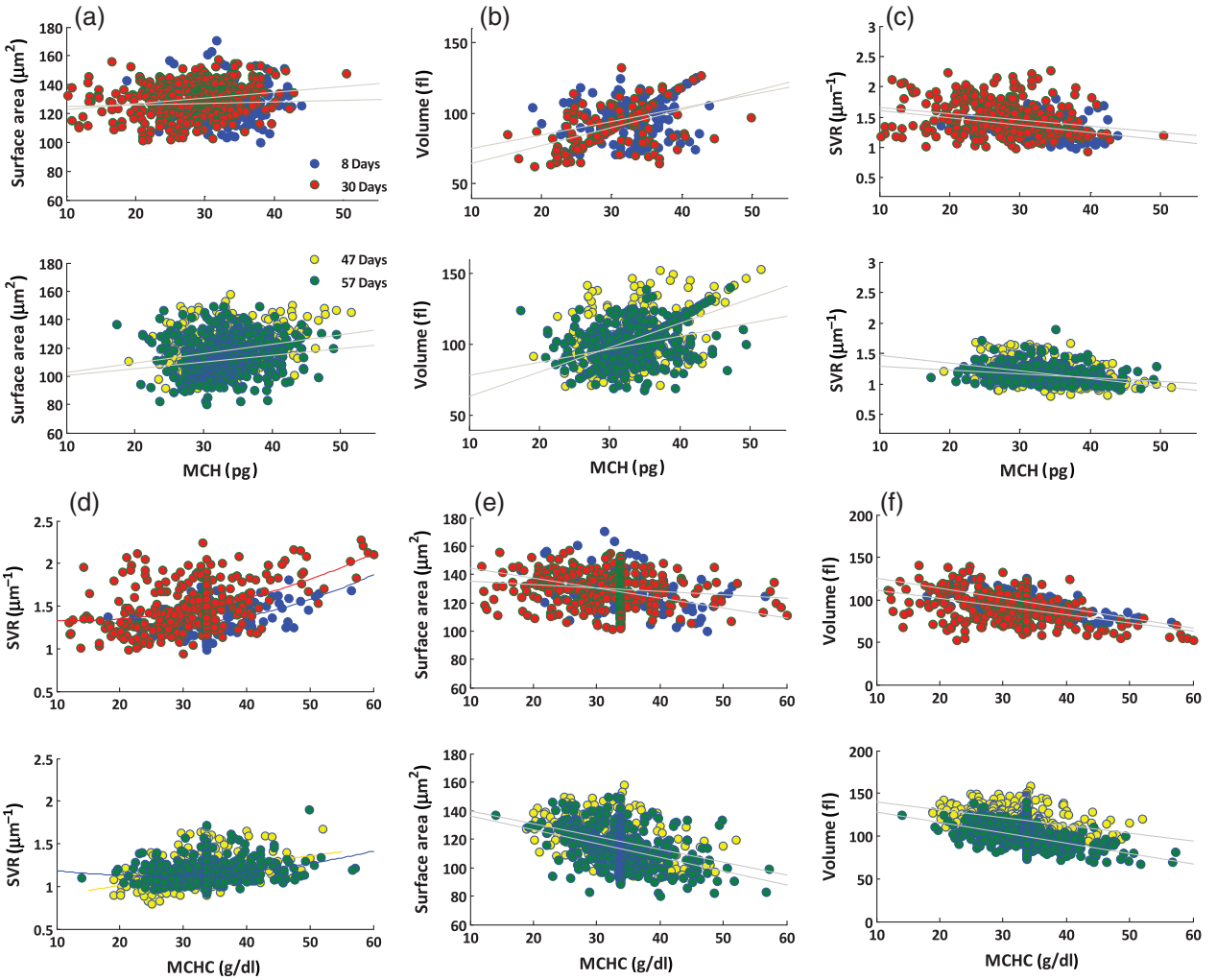

Fig. 6 Correlation between chemical-morphological and morphological–morphological properties (the gray lines show the linear relationship): (a) surface area and MCH, (b) volume and MCH, (c) SVR and MCH, (d) SVR and MCHC, (e) surface area and MCHC, and (f) volume and MCHC.

Table 2 Correlation results between the RBCs' geometrical parameters.

	Storage time (days)										
Property	8	13	16	23	27	30	34	37	40	47	57
Surface area versus diameter	0.7109	0.6722	0.5783	0.6145	0.6228	0.5105	0.6974	0.6513	0.7086	0.7162	0.5780
Volume versus diameter	0.2582	0.3331	0.3518	0.283	0.4336	0.1413	0.272	0.1476	0.1679	0.2726	0.2331
Volume versus surface area	0.4127	0.4617	0.5589	0.5433	0.5882	0.4701	0.6064	0.4071	0.4874	0.5449	0.6359

RBCs need to be deformable, so that they can stretch as they undergo distortions under mechanical stress during their circulation through narrow channels. However, spherocytes with less surface area suffer from less deformability. In addition to this, the viscosity of the spherocytic cells is higher than that of the biconcave RBCs, which causes high resistance during their passage through narrow channels.[47] The findings in this paper show that RBCs dominantly become spherocytes, lose surface area, and are around 20% and less deformable as their storage time exceeds 5 weeks.

4 Conclusion

We have estimated the 3-D geometric quantities related to the shape, type, and functionality of RBCs in storage lesion using DHM. Interestingly, the surface area values measured through our method are in approximate agreement with the surface area reported by the other techniques in the past. In addition, the 3-D geometric changes of RBCs in storage lesion have been investigated using the surface area value of RBCs. The investigation into the sphericity coefficient and morphological functionality factor along with the sphericity index shows that RBCs transform from biconcave to spherical as the storage time exceeds 5 weeks. Our experimental results demonstrate that the transition from biconcave to spherocyte is accompanied by a significant loss of surface area in an increase in the sphericity index. In addition, we conducted correlation analysis between chemical and morphological properties. It shows that the surface area has significant negative correlation with MCHC value. Interestingly, sphericity index has no correlation with either MCH or MCHC value similar to the functionality factor. Furthermore, correlation between surface area and diameter is stronger than volume and diameter.

Acknowledgments

This research was supported by Basic Science Research Program through the National Research Foundation of Korea (NRF) funded by the Ministry of Science, ICT & Future Planning (NRF-2013R1A2A2A05005687 and NRF-2015K1A1A2029224). We thank Daniel Boss and Pierre Marquet from Ecole Polytechnique Fédérale de Lausanne (EPFL), Switzerland, for their help with the experiments.

References

1. P. Canham, "The minimum energy of bending as a possible explanation of the biconcave shape of the human red blood cell," *J. Theor. Biol.* **26**(1), 61–81 (1970).
2. C. Uzoigwe, "The human erythrocyte has developed the biconcave disc shape to optimise the flow properties of the blood in the large vessels," *Med. Hypotheses* **67**, 1159–1163 (2006).
3. Z. Tu, "Geometry of membranes," *J. Geom. Symmetry Phys.* **24**, 45–75 (2011).
4. R. Card, "Red cell membrane changes during storage," *Transfus. Med. Rev.* **2**(1), 40–47 (1988).
5. S. Robinson et al., "Red blood cell storage duration and mortality in patients undergoing percutaneous coronary intervention," *Am. Heart J.* **159**(5), 876–881 (2010).
6. K. Alfano and M. Tarasev, "Investigating direct non-age metrics of stored blood quality loss," *Internet J. Med. Technol.* **5**(1), 1–9 (2008).
7. J. Laurie, D. Wyncoll, and C. Harrison, "New versus old blood—the debate continues," *Crit. Care* **14**(2), 130 (2010).
8. A. Alessandro et al., "Red blood cell storage: the story so far," *Blood Transfus.* **8**(2), 82–88 (2010).
9. C. Aubron et al., "Age of red blood cells and transfusion in critically ill patients," *Ann. Intensive Care* **3**(2), 1–11 (2013).
10. G. Bosman et al., "Erythrocyte ageing in vivo and in vitro: structural aspects and implications for transfusion," *Transfus. Med.* **18**(6), 335–347 (2008).
11. J. Goodman and R. Lawrence, "Digital image formation from electronically detected holograms," *Appl. Phys. Lett.* **11**(3), 77–79 (1967).
12. L. Onural and P. Scott, "Digital decoding of in-line holograms," *Opt. Eng.* **26**(11), 261124 (1987).
13. U. Schnars, "Direct phase determination in hologram interferometry with use of digitally recorded holograms," *J. Opt. Soc. Am. A* **11**(7), 2011–2015 (1994).
14. D. Carl et al., "Parameter-optimized digital holographic microscope for high-resolution living-cell analysis," *Appl. Opt.* **43**(36), 6536–6544 (2004).
15. C. Wagner, W. Osten, and S. Seebacher, "Direct shape measurement by digital wavefront reconstruction and multi-wavelength contouring," *Opt. Eng.* **39**(1), 79–85 (2000).
16. Y. Zhang et al., "Reconstruction of in-line digital holograms from two intensity measurements," *Opt. Lett.* **29**(15), 1787–1789 (2004).
17. Y. Frauel et al., "Three-dimensional imaging and processing using computational holographic imaging," *Proc. IEEE* **94**(3), 636–653 (2006).
18. F. Merola et al., "Digital holography as a method for 3D imaging and estimating the biovolume of motile cells," *Lab Chip* **13**(23), 4512–4516 (2013).
19. I. Moon et al., "Automated three dimensional identification and tracking of micro/nano biological organisms by computational holographic microscopy," *Proc. IEEE* **97**, 990–1010 (2009).
20. F. Dubois et al., "Digital holographic microscopy for the three-dimensional dynamic analysis of in vitro cancer cell migration," *J. Biomed. Opt.* **11**(5), 054032 (2006).
21. M. Kim, *Digital Holographic Microscopy*, Springer, New York (2011).
22. A. Mallahi, C. Minetti, and F. Dubois, "Automated three-dimensional detection and classification of living organisms using digital holographic microscopy with partial spatial coherent source: application to the monitoring of drinking water resources," *Appl. Opt.* **52**, A62–A80 (2013).
23. K. Alm et al., *Digital Holography and Cell Studies*, In Tech, Croatia (2011).
24. I. Moon et al., "Automated quantitative analysis of 3D morphology and mean corpuscular hemoglobin in human red blood cells stored in different periods," *Opt. Express* **21**(25), 30947–30957 (2013).
25. Y. Kim et al., "Profiling individual human red blood cells using common-path diffraction optical tomography," *Sci. Rep.* **4**, 1–7 (2014).

26. B. Bhaduri et al., "Optical assay of erythrocyte function in banked blood," *Sci. Rep.* **4**, 1–6 (2014).
27. F. Yi et al., "Automated segmentation of multiple red blood cells with digital holographic microscopy," *J. Biomed. Opt.* **18**(2), 026006 (2013).
28. G. Tomaiuolo et al., "Comparison of two flow-based imaging methods to measure individual red blood cell area and volume," *Cytometry A* **81**(12), 1040–1047 (2012).
29. E. Evans and Y. Fung, "Improved measurements of the erythrocyte geometry," *Microvasc. Res.* **4**(4), 335–347 (1972).
30. R. Waugh et al., "Rheologic properties of senescent erythrocytes: loss of surface area and volume with red blood cell age," *Blood* **79**(5), 1351–1358 (1992).
31. P. Marquet et al., "Digital holographic microscopy: a noninvasive contrast imaging technique allowing quantitative visualization of living cells with sub wavelength axial accuracy," *Opt. Lett.* **30**(5), 468–470 (2005).
32. E. Cuche, P. Marquet, and C. Depeursinge, "Simultaneous amplitude and quantitative phase contrast microscopy by numerical reconstruction of Fresnel off-axis holograms," *Appl. Opt.* **38**, 6994–7001 (1999).
33. T. Colomb et al., "Automatic procedure for aberration compensation in digital holographic microscopy and application to specimen shape compensation," *Appl. Opt.* **45**, 851–863 (2006).
34. B. Rappaz et al., "Comparative study of human erythrocytes by digital holographic microscopy, confocal microscopy, and impedance volume analyzer," *Cytometry A* **73**(10), 895–903 (2008).
35. B. Rappaz et al., "Simultaneous cell morphometry and refractive index measurement with dual-wavelength digital holographic microscopy and dye-enhanced dispersion of perfusion medium," *Opt. Lett.* **33**(7), 744–746 (2008).
36. T. Tishko, T. Dmitry, and T. Vladimir, *Holographic Microscopy of Phase Microscopic Objects*, World Scientific, New Jersey (2011).
37. W. Kaplan, *Advanced Calculus*, Addison-Wesley, Reading, MA (1992).
38. L. Cesari, *Surface Area*, Princeton University Press, New Jersey (1956).
39. B. Rappaz et al., "Noninvasive characterization of the fission yeast cell cycle by monitoring dry mass with digital holographic microscopy," *J. Biomed. Opt.* **14**(3), 034049 (2009).
40. P. Canham and A. Burton, "Distribution of size and shape in populations of normal human red cells," *Circ. Res.* **22**(3), 405–422 (1968).
41. Y. Park et al., "Measurement of red blood cell mechanics during morphological changes," *Proc. Natl. Acad. Sci. U. S. A.* **107**(15), 6731–6736 (2010).
42. J. Bronzino, *The Biomedical Engineering Handbook*, CRC Press, Boca Raton (2000).
43. K. Tachev, K. Danov, and P. Kralchevsky, "On the mechanism of stomatocyte-echinocyte transformations of red blood cells: experiment and theoretical model," *Colloids Surf., B* **34**(2), 123–140 (2004).
44. I. Moon et al., "Automated statistical quantification of three-dimensional morphology and mean corpuscular hemoglobin of multiple red blood cells," *Opt. Express* **20**(9), 10295–10309 (2012).
45. X. Long et al., "Correlation analysis between mean corpuscular hemoglobin and mean corpuscular volume for thalassemia screening in large population," *Am. J. Anal. Chem.* **5**, 901–907 (2014).
46. G. Rao, L. Morghom, and S. Mansori, "Negative correlation between erythrocyte count and mean corpuscular volume or mean corpuscular haemoglobin in diabetic and non-diabetic subjects," *Horm. Metab. Res.* **17**(10), 540–541 (1985).
47. Y. Yawata, *Cell Membrane: The Red Blood Cell as a Model*, Wiley-VCH Verlag, Weinheim, Germany (2004).

Keyvan Jaferzadeh is a PhD student in the Computer Engineering Department of Chosun University, Republic of Korea. He received his BS degree in software engineering in 2006 and his MS degree in mechatronics engineering in 2010. His current research interests include image processing, digital holography, image compression, and machine vision.

Inkyu Moon received his BS degree in electronics engineering from SungKyunKwan University, Republic of Korea, in 1996 and his PhD in electrical and computer engineering from the University of Connecticut, United States, in 2007. He joined Chosun University in Korea in 2009 and is currently an associate professor at the School of Computer Engineering there. His research interests include digital holography, biomedical imaging, and optical information processing. He is a member of IEEE, OSA, and SPIE.